Supporting Information

Antitumor therapeutic application of self-assembled RNAi-AuNP nanoconstructs; Combination of VEGF-RNAi and photothermal ablation

By

Sejin Son et al.

Contents of Supporting Information

Fig. S1. Optimization of PEI/RNAi-AuNP formulation parameters in terms of hydrodynamic size (a) and UV-VIS absorption spectrum (b) with varying N/P ratios.

Fig. S2. TEM images of various geometries of RNAi-AuNPs with PEI complexation. Spherical RNA-AuNP with PEI (a, b, d), ring-like RNAi-AuNP (c,e) and dumbell-like RNAi-AuNP (f).

Fig. S3. UV-VIS spectrum of various geometries of RNAi-AuNPs with PEI polymer.

Fig. S4. Dark field images of PC cells with bioreducible PEI/RNAi-AuNPs (a,b) and non-reducible PEI/RNAi-AuNPs (c,d) at N/P ratio of 30 after 6 h incubation.

Fig. S5. Time dependent VEGF gene silencing efficacy of monomeric and dimeric siVEGF with PEI formulations. All formulations were formed at N/P ration of 30.

Fig. S6. In vitro siVEGF gene silencing efficacy by measuring VEGF protein level (left) and western blotting analysis (right) after 48 h transfection with varying formulations in comparison with scrambled siRNA-AuNP.

Fig. S7. Histological examination (H&E staining) of therapeutic efficacy by anti-VEGF and photothermal combination therapy. Yellow arrows are indicative of blood vessels in tumor tissue.

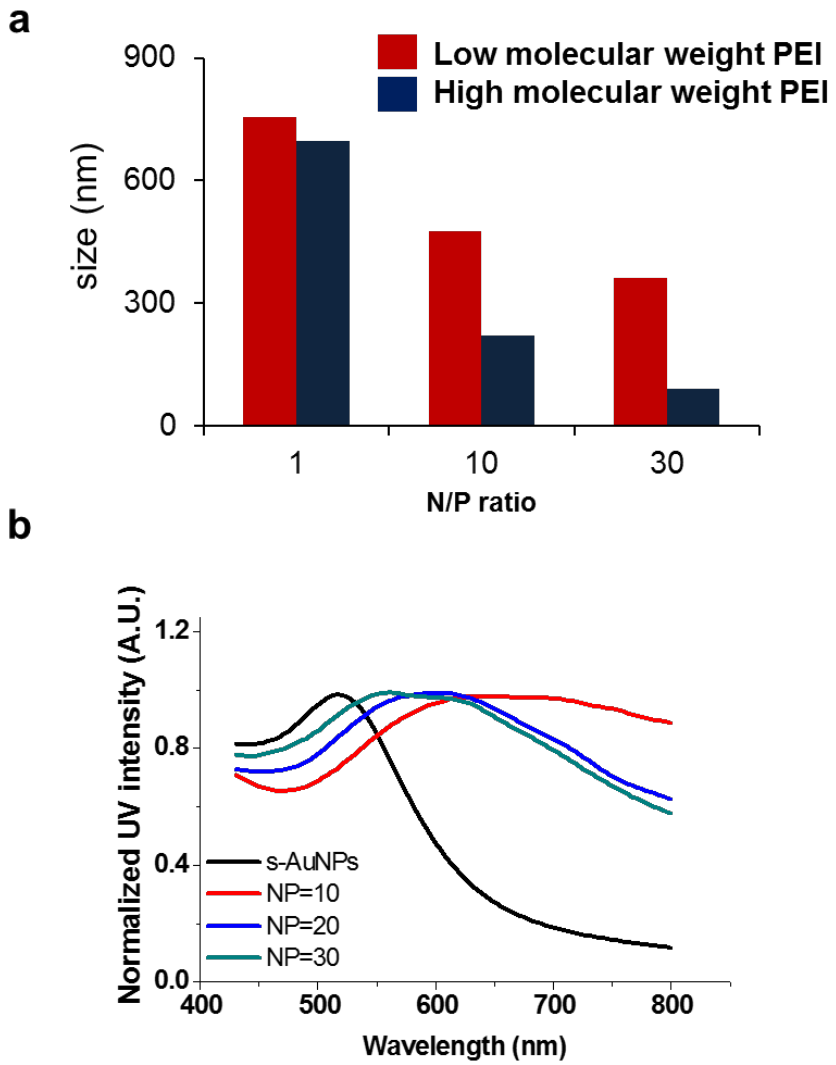

Fig S1. Optimization of PEI/RNAi-AuNP formulation parameters in terms of hydrodynamic size (a) and UV-VIS absorption spectrum (b) with varying N/P ratios

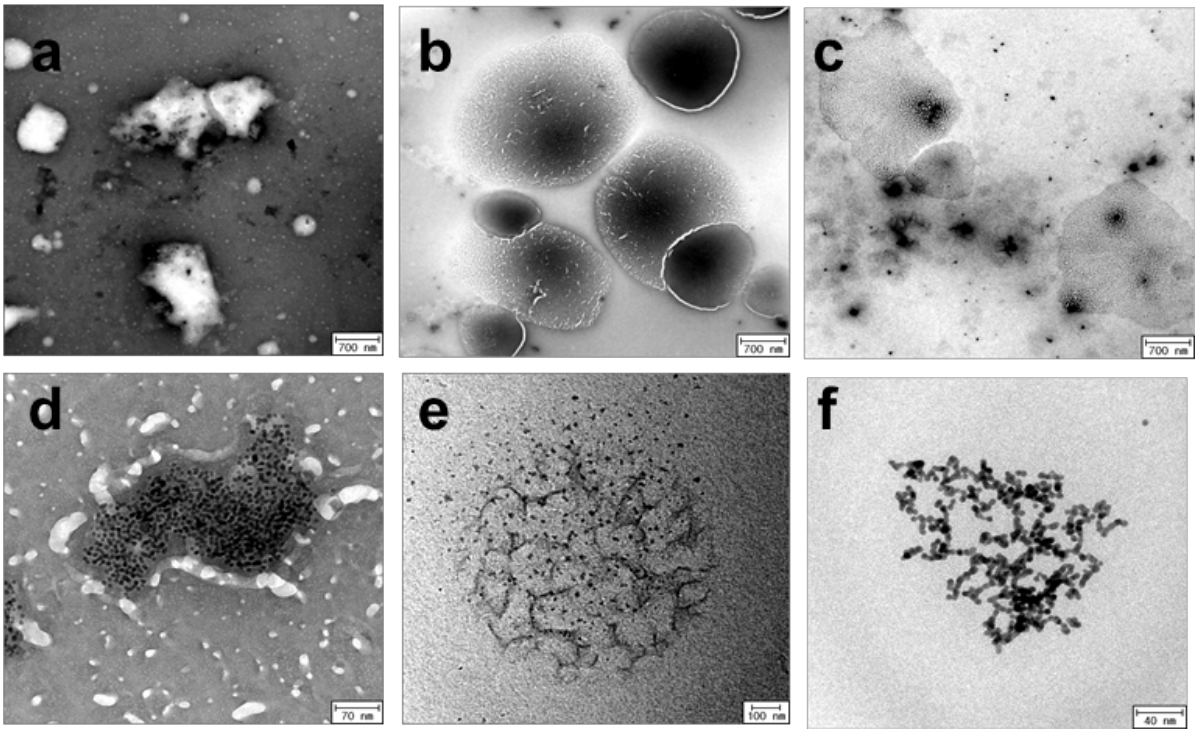

Fig. S2. TEM images of various geometries of RNAi-AuNPs with PEI complexation. Spherical RNA-AuNP with PEI (a, b, d), ring-like RNAi-AuNP (c,e) and dumbell-like RNAi-AuNP (f).

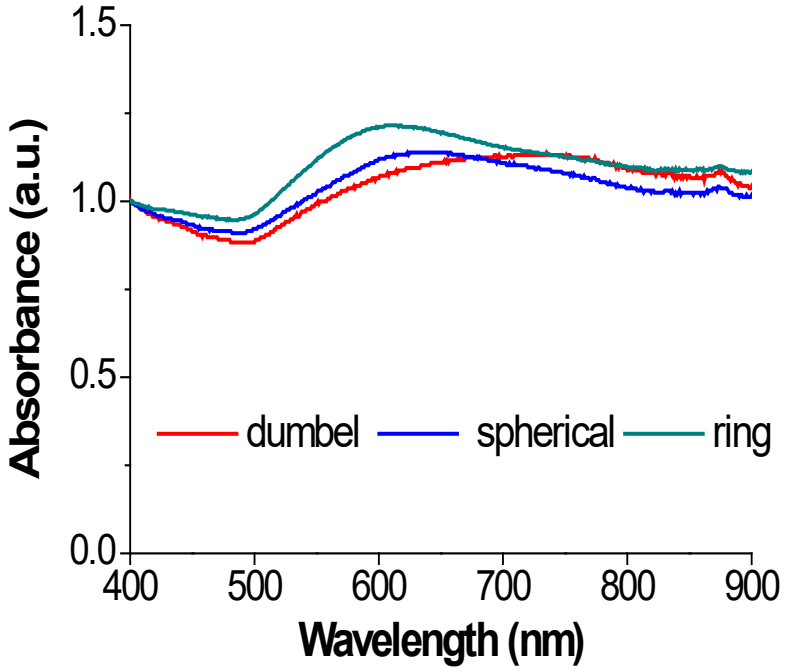

Fig. S3. UV-VIS spectrum of various geometries of RNAi-AuNPs with PEI polymer.

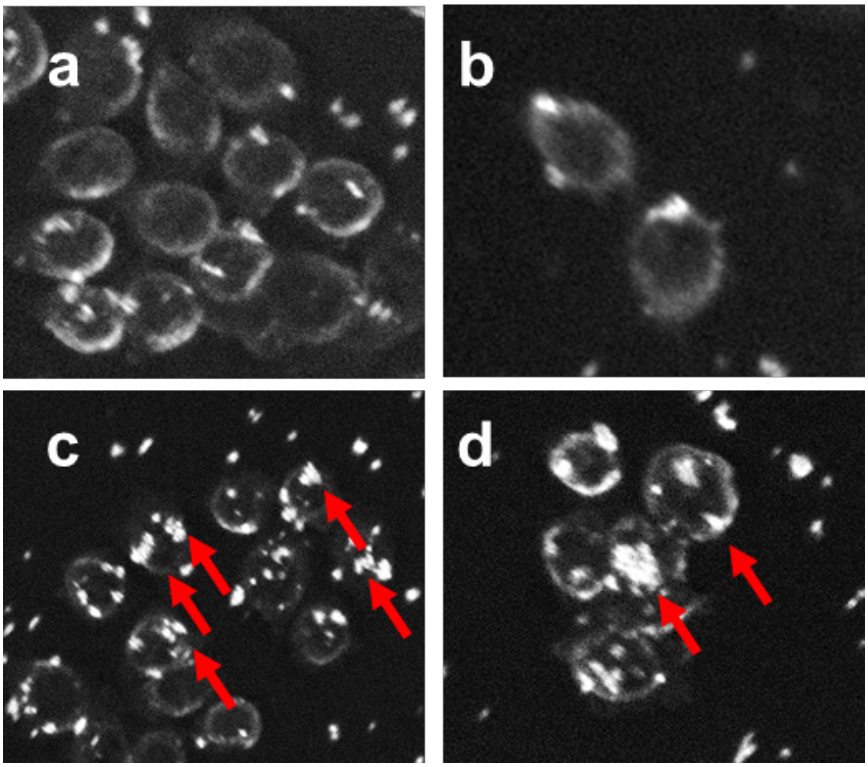

Fig. S4. Dark field images of PC cells with bioreducible PEI/RNAi-AuNPs (a,b) and non-reducible PEI/RNAi-AuNPs (c,d) at N/P ratio of 30 after 6 h incubation.

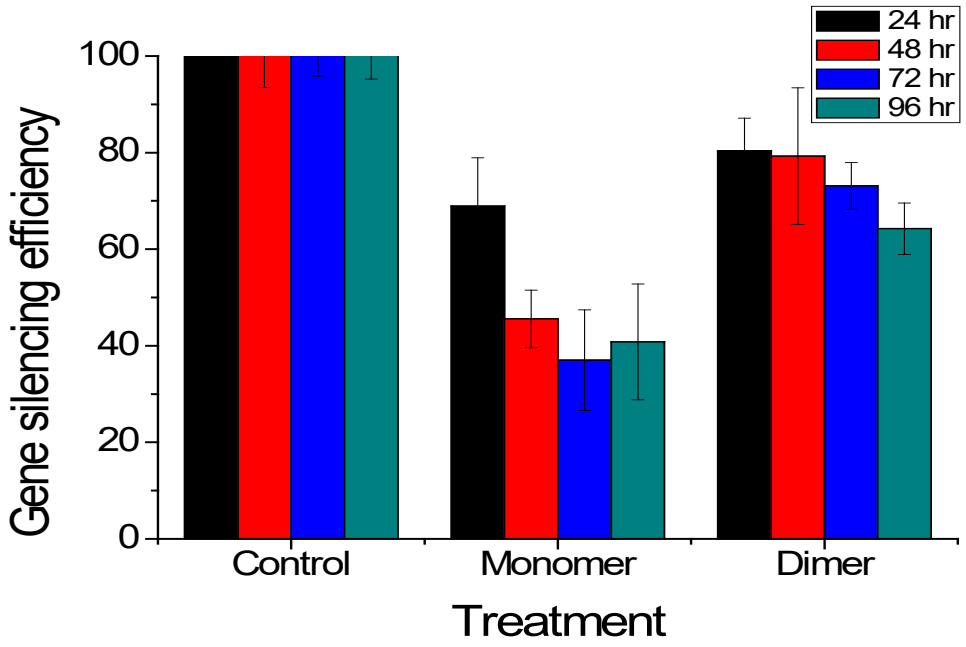

Fig. S5. Time dependent VEGF gene silencing efficacy of monomeric and dimeric siVEGF with PEI formulations. All formulations were formed at N/P ration of 30.

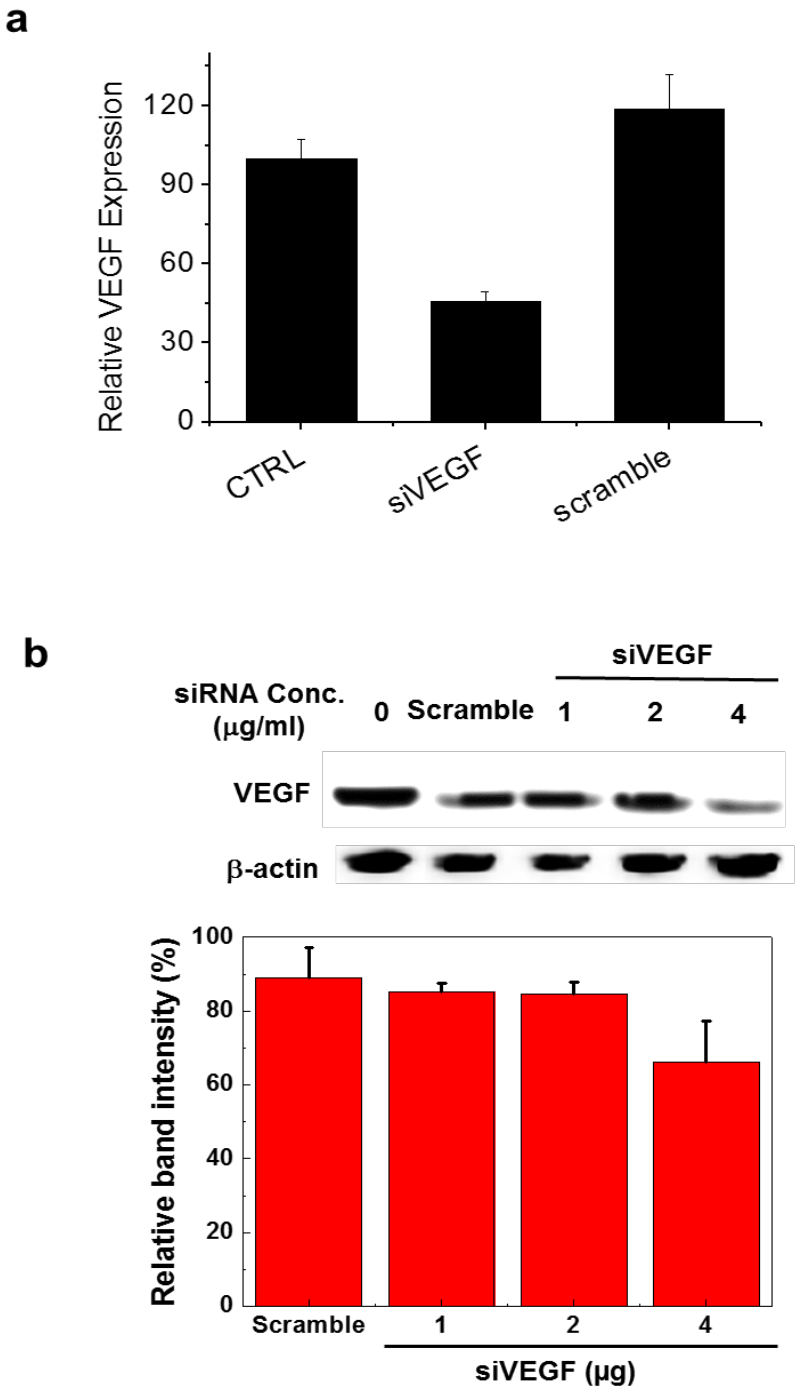

Fig. S6. In vitro siVEGF gene silencing efficacy by measuring VEGF protein level (left) and western blotting analysis (right) after 48 h transfection with varying formulations in comparison with scrambled siRNA-AuNP.

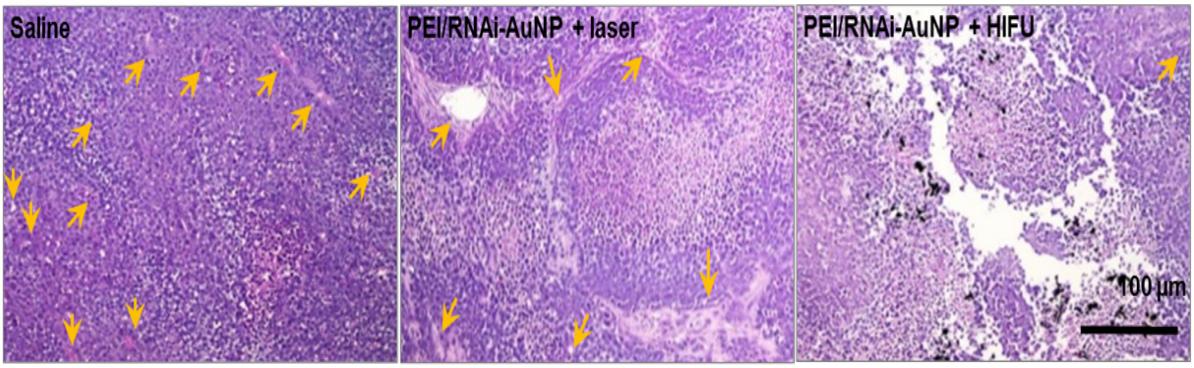

Fig. S7. Histological examination (H&E staining) of therapeutic efficacy by anti-VEGF and photothermal combination therapy. Yellow arrows are indicative of blood vessels in tumor tissue.